Eur. Phys. J. D **29**, 39–47 (2004)
DOI: 10.1140/epjd/e2004-00002-x

THE EUROPEAN PHYSICAL JOURNAL D

Influence of electronic and geometric properties on melting of sodium clusters

K. Manninen[a], A. Rytkönen, and M. Manninen

NanoScience Center, Department of Physics, PB 35 (YFL), University of Jyväskylä, 40014 Jyväskylä, Finland

Received 10 September 2003 / Received in final form 30 October 2003
Published online 20 January 2004 –

Abstract. Systematics of the melting transition for sodium clusters with 40–355 atoms has been studied with both ab initio and semiclassical molecular dynamics simulations. The melting temperatures obtained with an ab initio method for Na_{55}^+ and Na_{93}^+ correlate well with the experimental results. The semiclassically determined melting temperatures show similarities with the experimentally determined ones in the size region from 55 to 93 and near size 142, and the latent heat in the size region from 55 to 139, but not elsewhere in the size region studied. This indicates that the nonmonotonical melting behavior observed experimentally cannot be fully explained by geometrical effects. The semiclassically determined melting temperature and the latent heat correlate quite well, indicating that they respond similarly to changes in cluster geometry and size. Similarly, the binding energy per atom seems to correlate with the melting temperature and the latent heat of fusion.

PACS. 36.40.Ei Phase transitions in clusters

1 Introduction

Usually clusters melt at temperatures lower than bulk because of their high proportion of surface atoms with reduced binding energy. This has been observed both in theoretical simulations [1,2] and in experiments [3–5]. Exceptions also exist: Shvartsburg and Jarrold [6] demonstrated that small tin clusters ions with 10−30 atoms remain solid above melting temperature of bulk tin. Nevertheless, in general, as the cluster size decreases, the melting temperature and latent heat of fusion per atom decrease and the melting transition region widens [1,7]. For example, the melting temperatures of tin clusters decrease systematically as the size of the cluster decreases from 50 to 5 nm [1]. Rytkönen et al. [8] estimated the melting temperatures for sodium clusters in the size range $N = 8-55$ using an ab initio simulation method and found that they decrease nearly monotonically as a function of size. However, because almost all sizes studied were electronically magic, these calculations do not exclude the possibility for nonmonotonical behavior. There is indeed evidence indicating that the melting temperatures of sodium clusters do not vary monotonically with cluster size for clusters small enough (<350 atoms) [7,9–11]. Nonmonotonical melting temperature variation has been observed in numerical experiments also for argon clusters [12].

The melting transition of a finite cluster does not occur at a well defined temperature as in the bulk. Instead, the melting transition spreads over a finite temperature region, and the temperature range broadens as the cluster size decreases [13,14]. The freezing temperature T_f is generally defined to be the lower end of the melting temperature range below which the cluster is completely solid and, respectively, the upper end of the range defines the melting temperature T_{melt} above which the cluster is in a completely liquid phase.

Between T_f and T_{melt}, clusters show premelting, structural isomerization [7,15], and dynamical coexistence. The most usual premelting case is surface melting [16–18]. Surface melting of a cluster occurs over a broad temperature range, whereas homogeneous melting of the solid core occurs abruptly [19]. Clusters small enough also exhibit dynamical coexistence where the cluster can fluctuate in time between solid and liquid phase [16,20–24], so an ensemble of clusters is a mixture of low-energy (solid) and high-energy (liquid) forms. In the coexistence region, where both solid-like and liquid-like states can occur, the energy as a function of temperature may exhibit an S-shaped curvature. The curve is called the caloric curve and its derivative, $C(T) = \partial E/\partial T$, the heat capacity.

There are a number of methods how melting transition can be detected and the melting temperature determined. Melting transition of a cluster is commonly characterized by a broad peak in the heat capacity instead of the usual delta function in the bulk [3,5,11,13]. One possibility to define the melting temperature is to identify the temperature of the maximum heat capacity as the melting

[a] e-mail: kirsi.manninen@phys.jyu.fi

point [3,5,10,11,13,25], or equivalently a steep rise in the potential energy versus temperature curve [1,2,4,19,26]. Melting temperature of the cluster can also be determined from the mean square displacement (MSD) as a function of temperature [2,7,27]. In the case of the MSD, it is not so easy to define the temperature where we can say that the cluster melts [28]. One possibility is Lindemann's criterion [29,30], stating that melting happens when the root-mean-square displacement (for a relatively short time interval) for the atoms of the cluster reaches a critical fraction ($\delta > 0.1$) of the distances between them. The melting temperature has in some cases been taken as half the value of the coexistence interval, $(T_f+T_{melt})/2$ [21], and in some cases as the value T_{melt} [19].

The first experimental study of the melting temperatures of sodium clusters has been performed by Martin et al. [31]. The disappearance of the geometric shell structure in mass spectra of sodium clusters as the cluster ensemble is heated was used as a criterion for melting in this study. In general, the melting behavior was monotonical as a function of cluster size. With this method, however, no information could be extracted on the melting behavior between the geometrically magic sizes. After that, a measurement of the melting temperatures has been performed by Haberland and collaborators [3,11,13]. In this work, the melting temperatures of sodium cluster cations were deduced from caloric curves obtained from photodissociation measurements. According to these measurements, the melting temperature is not a monotonically increasing function of cluster size. In particular, the melting temperature of Na_{55}^+ was found to be higher than the ones for the other sizes in the range $N < 350$ atoms. The melting temperature as a function of cluster size show also a pronounced peak of the melting temperature at $N = 142$.

A number of computer simulations on melting in small sodium clusters has been reported. The majority of the simulations has been performed using phenomenological interatomic potentials [7,23,32–36]. Other simulation type include ab initio methods [2,37–39], which allow a more realistic treatment, but are computationally much more expensive than the ones performed using phenomenological potentials. Calvo and Spiegelmann [10] employed a classical empirical potential (they used an abbreviation SMA), which is the same as we used in our semiclassical calculations, and a simple tight-binding model (TB) to study the size range $N = 8-147$. They observed that for less than 75 atom clusters, both the melting temperature and the latent heat of melting exhibit strong, nonmonotonic variations as a function of size. For large sizes, the transition was found to resemble the bulk solid-liquid phase transition rounded by finite size effects. Rytkönen et al. [2] used ab initio molecular dynamics simulations to study the dynamics and electronic structure of Na_{55}. The melting transition was observed in the region 300−350 K with latent heat of melting 11 meV/atom. Aguado et al. [37,38] performed constant energy molecular dynamics simulations with the Car-Parrinello technique using semiclassical density functional theory. Surface melting was observed at ∼240 K for Na_{142}, homogeneous melting at ∼270 K, and for Na_{92}, respectively, at ∼130 K and ∼240 K. Na_{55} was observed to melt at 190 K.

Table 1. The melting temperature, the latent heat of fusion and the width of the transition region as a function of cluster size.

N	T_{melt} [K]	L [meV/atom]	width [K]
55	162	8.3	26
93	133	4.2	31
110	147	6.1	15
120	183	7.9	18
139	186	11.8	8
142	186	12.1	2
147	176	11.1	4
168	173	7.9	15
184	175	8.1	15
193	184	9.4	14
215	180	10.0	20
247	193	11.2	9
271	214	13.8	9
279	214	8.8	2
299	211	14.5	3
309	204	22.3	8
339	203	12.3	9
345	194	11.5	20
355	202	11.4	8

It has been experimentally observed that for large sodium clusters, the peaks in the mass spectrum correspond to icosahedral shell closings [40]. For small sodium clusters, the peaks of the mass spectrum have been observed to correspond to electronic shell closings [5]. Because of the electronic contribution, the binding energy per atom reaches a maximum at electronic shell closings [41]. However, the large fluctuations in the experimentally determined melting temperatures are not correlated with either electronic or geometric shell closings, and consequently the fluctuation in the melting temperature against the number of atoms can not be directly explained in terms of either of these quantities.

Experimentally, it has been observed that the latent heat of fusion decreases from the bulk value when the cluster size is decreased [1]. Molecular dynamics simulations have also shown a steady decrease in latent heat of fusion with decreasing cluster size for gold clusters [4]. Kusche et al. [13] have studied the variation of the latent heat and they found out that the maxima occur near, but not at the same sizes as for T_{melt} and the peaks in the latent heat seem to be shifted from that of T_{melt} in the direction of the icosahedral shell closings.

The width of phase transitions in finite systems has not been studied systematically. Imry [42] has shown that the broadening of a first-order phase transition is proportional to the latent heat of the transition. Similar findings were made by Labastie and Whetten [43].

The binding energy has been calculated for small ($2 \leq N \leq 14$) sodium clusters using both ab initio and classical molecular dynamics simulations [44]. The binding

energy values calculated with the classical model are 0.15−0.20 eV higher than the ones calculated with the ab initio method. They also increase monotonically and approach the bulk sodium value already at $N = 13$. Rey et al. [45] studied the binding energies of Ni_N, Pd_N, Au_M, and Ag_N clusters ($N = 2-23$) on the basis of the embedded-atom model and the second-moment approximation to the tight-binding method using constant-energy molecular dynamics simulations. The calculated binding energies increase monotonically as the size of the cluster increases. Northby et al. [46] pointed out that the most tightly bound Lennard-Jones cluster in the size range $13 \leq N \leq 147$ is $N = 135$. This structure is a truncated 147-atom icosahedron without its 12 corner atoms. The binding energy differences showed also that the binding energy per atom increases linearly in the size range $136 \leq N \leq 147$.

The aim of our work is to study the mechanisms by which the large fluctuations in the melting temperature of metal clusters are caused. In this paper, we present the results from both semiclassical and ab initio molecular-dynamics (MD) simulations of sodium clusters with both magic and nonmagic numbers of atoms. Using the ab initio method, we find melting temperatures in good agreement with the experimental results [3,5,11] for Na_{55}^+ and Na_{93}^+. With the semiclassical method, similarities were found for sizes $N < 150$ for both melting temperature and latent heat of melting, but not for the larger sizes. This indicates that simple model potential calculations do not offer an explanation for the nonmonotonical behavior but more sophisticated methods are needed.

2 Simulation methods

Caloric curves for cluster sizes $N = 40-355$ were calculated with semiclassical molecular dynamics simulations carried out using the Verlet algorithm for time-integration of the equations of motion [47]. The Nosé-Hoover thermostat [48] with time constant $\tau = 25$ fs was used to derive results valid for the canonical ensemble. We used the time step 5 fs. The system was run for 0.5 ns to achieve equilibrium at a specific temperature and 5 ns for extracting the data.

For our simulations, we chose an empirical many-body potential

$$V = -\sum_{i=1}^{N} \left\{ \sqrt{\sum_{j=1\neq i}^{N} \zeta_0^2 \exp\left[-2q\left(\frac{r_{ij}}{r_0} - 1\right)\right]} - \sum_{j=1\neq i}^{N} \epsilon_0 \exp\left[-p\left(\frac{r_{ij}}{r_0} - 1\right)\right] \right\}, \quad (1)$$

where $\epsilon_0 = 15.956$ meV, $\zeta_0 = 291.14$ meV, $r_0 = 6.99a_0$, $q = 1.30$ and $p = 10.13$. The form and the parameters are those given by Li et al. [49].

Several (from 17 to 35) constant temperature molecular dynamics simulations were performed for each cluster size to obtain the caloric curve. The initial configurations for all the simulations were icosahedral geometries. Nonmagic clusters were prepared by removing surface atoms from a cluster with a magic number. The cluster sizes studied were chosen to correspond to a local minimum or maximum of the experimentally measured curve [3,11,13]. Total and potential energies as well as heat capacities were used to analyse the transition from solid to liquid phase. The melting temperature of the cluster was determined to be at the temperature where the heat capacity curve attains its maximum value.

For each cluster size we determined the energy of the cluster versus its temperature. Because of the limited number of simulations for one single cluster and statistical fluctuation in energy, we fitted a monotonous function to the simulation data. The total energy at any temperature in the ensemble was estimated by

$$E_{tot}(T) = f(T)C_{sol}(T) + [1 - f(T)]C_{liq}(T) \quad (2)$$

where

$$C_{sol}(T) = a_{sol} + b_{sol}T \quad (3)$$

$$C_{liq}(T) = a_{liq} + b_{liq}T \quad (4)$$

and $f(T)$ is given by

$$f(T) = \frac{1}{e^{(T-T_0)/c} + 1}. \quad (5)$$

$f(T)$ and $1 - f(T)$ represent the fraction of time spent in the solidlike and the liquidlike phases, respectively. Because E_{tot} curves for the solidlike and the liquidlike phases were assumed to be linear outside the coexistence range, a least-squares fit of points gives the constants a_{sol}, b_{sol}, a_{liq}, b_{liq}, T_0 and c. c shows how abrupt the transition is, and T_0 is maximum point of the heat capacity. Now the heat capacity can be directly extracted by taking the derivative of E_{tot} with respect to T, and the melting temperature T_{melt} extracted as the temperature where the heat capacity attains its maximum value, which is T_0. Our method is thus analogous to the one employed by Schmidt et al. [5,11]. Values of the latent heat of fusion have been obtained by extrapolating the lines corresponding to solidlike and liquidlike phases (Eqs. (3, 4)) to the region in between and determining the energy difference between these lines at $T = T_{melt}$.

The ab initio calculations were performed using a BO-LSD-MD (Born-Oppenheimer local-spin-density molecular dynamics) simulation method devised by Barnett and Landman [50]. Since the ab initio MD method used is fully documented in reference [50], we just give here a brief review of the computational method.

In this method, the full electronic structure calculation is done explicitly for the sodium $3s^1$ electrons with norm-conserving nonlocal pseudopotentials and a plane-wave basis set [51,52]. The Kohn-Sham one-electron equations are solved at each time step using the LDA approximation to get the valence electron density. For each nuclear configuration, the Hellmann-Feynman forces on the ions

are calculated from the converged solution of the valence electron density, so the total forces on the ions are these forces together with the Coulomb repulsion of the positive ion cores.

In the case of Na_{93}^+, the initial configuration for the simulation was a structure based on the icosahedron. Several different structures were optimized to a local minimum and the energetically most favorable one was chosen as the starting configuration. An ab initio molecular dynamics simulation was performed at three different total energies corresponding to average temperatures 248 K, 262 K, and 274 K. The cluster was first equilibrated for 1 ps and the dynamics of the cluster was monitored for 1 ps at each total energy using time step 1 fs. Several indicators, for example the diffusion coefficient, were used to determine the phase of the cluster at each total energy. With this information, an estimation for the melting temperature for Na_{93}^+ could be determined.

The results for Na_{55}^+ are extracted from reference [39]. The simulation was started from a ionic configuration corresponding to a perfect icosahedron. The cluster was heated at a constant rate of 5 K/ps, and the energy vs. temperature curves were plotted. From these curves, the melting temperature region and the latent heat of melting could be extracted as from a caloric curve. Details of the method can be found for example in references [2,39].

3 Results

Semiclassical simulations were performed for selected cluster sizes in the region $N = 40-355$. Almost all selected cluster sizes are near local minimum or maximum values of the experimentally determined melting temperature as a function of cluster size curve [3,11,13]. All cluster sizes except for Na_{40} satisfy the equation for $E_{tot}(T)$ (Eq. (2)) quite well. Because the melting temperature region of Na_{40} is fairly broad, the simulated data does not fit to equation (2).

Figure 1 shows three examples of the caloric curves made by using semiclassical MD. For comparison Figure 1b shows the potential energy as a function of temperature calculated using our ab initio method. The ab initio simulation of Na_{55}^+ is presented because it is the only one we could compare to semiclassical results. The cluster size Na_{168} is shown because this cluster size had the biggest problem in fitting the curve from equation (2). For sizes larger than 193 atoms, the caloric curves show a small increase near the freezing temperature T_f. The size (Na_{215}) is an example showing this increase. The cause of this is most likely surface melting, observed also previously for large clusters [19].

The statistical errors of our semiclassical simulations are relatively small as seen in Figure 1. However, for large cluster sizes, with more than 150 atoms, it is nearly impossible to find the geometry of the global minimum energy. Also, in this size region there could be several quite different geometries within a small energy interval. We use icosahedral starting geometries since we know that our model potential gives those as ground state geometries close to the complete icosahedra.

The melting temperature of sodium clusters determined experimentally [3,11,13], semiclassically, and with the ab initio method is presented in Figure 2 as a function of cluster size. The results of calculations made by Calvo et al. [10] are also presented in the same figure.

Our semiclassical results show maxima of the melting temperature are at cluster sizes $N = 55$, $139-142$, 193 and $271-279$. Geometrical shell closing numbers seem to correlate with the melting temperature behavior for clusters with less than 150 atoms, but not for the larger sizes. The melting temperature region obtained both semiclassically and with the ab initio method [2] for Na_{40} is also presented in Figure 2. Experimentally, the melting temperature for this size has not been determined due to the problems caused by broadening of the phase transition.

The experimental results exhibit similar kind of behavior for sizes from 55 to 93 and near size 142 as the one seen in our semiclassical results. However, for larger sizes, the experimental curve has more maxima, and these do not seem to correlate with ours. The overall temperature difference between the experimental and the simulation results is most likely caused by the difference between the bulk melting temperatures. The melting temperature of bulk for the semiclassical potential (Eq. (1)) used in our simulations is 332.9 K as instead the experimental melting temperature of bulk sodium is 370.1 K.

One could also mention that comparing with the results by Calvo and Spiegelmann [10], our melting temperatures are lower than those presented in reference [10]. The differences between the results are probably related to different simulation and analyzing methods. Calvo and Spiegelmann used Monte Carlo method with parallel tempering [54,55], while we use standard molecular dynamics.

Comparison of the experimental and our semiclassical results of Figure 2 seems to indicate that by using a phenomenological potential to describe the behavior of a simple metal, one can not reproduce the variations seen in the experimental melting temperature curve. Both curves are nonmonotonic, but the peaks are not clearly correlated in any size region. However, the melting temperatures extracted using the ab initio method seem to agree nicely with the experimental ones also quantitatively. This indicates that ab initio or corresponding treatment is needed in order to reproduce the experimental results. This means that the electronic structure plays an important role in the nonmonotonic variation of the melting temperature.

The simulations for Na_{93}^+ were performed in three different temperatures estimated to be close to the melting transition. Naturally, with help of only three points it is not possible to determine the caloric curve. Nevertheless, the solid or liquid phase can be quite reliably determined by comparing the diffusion constant with those determined for other cluster sizes. We have earlier estimated the melting temperature region of Na_{55}^+ using several different methods, including the caloric curve and the diffusion constants [8].

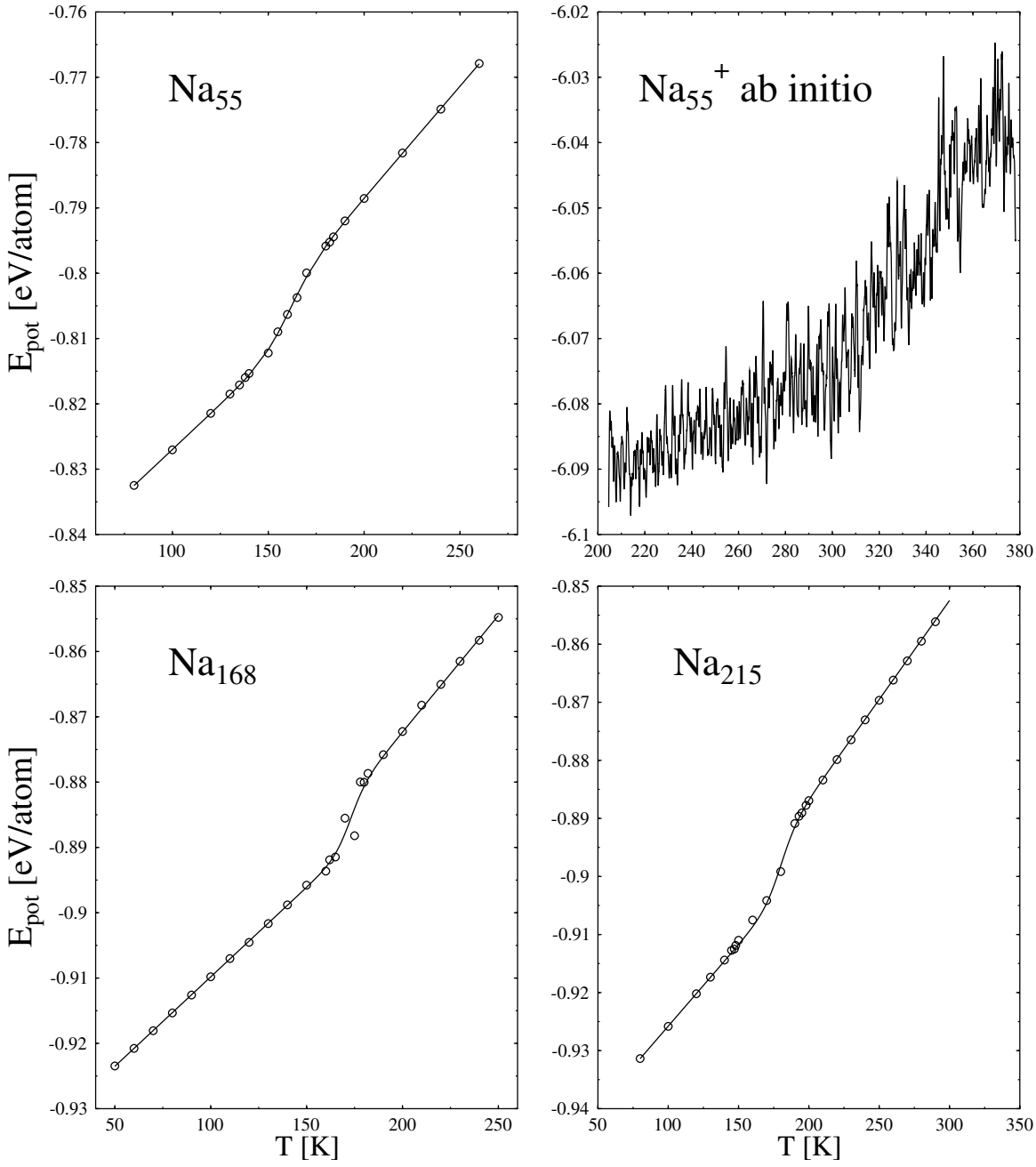

Fig. 1. Potential energy as a function of temperature. Open circles are results from constant temperature simulations with the semiclassical potential (the point size represents statistical errors). Solid lines show the fits to equation (2). The ab initio result shows the potential energy variation during heating with a thermostat.

The diffusion constant is calculated from the mean square displacement of the ions with respect to the positions of the ions ($D = (MSD)^2/6t$). The melting region may be interpreted to be when the diffusion constant starts to increase. When the cluster is solid the diffusion coefficient displays values lower than 0.3×10^{-5} cm^2/s [2]. The diffusion coefficient increases when the temperature is increased and the cluster is melted and finally the value for the diffusion coefficient reaches the bulk liquid sodium value, which is over 2×10^{-5} cm^2/s. In the case of Na_{55}^+ the diffusion constant was calculated over time periods of 4 ps and plotted as a function of the average temperature in each time periods.

The results for the diffusion constant are shown in Figure 3 together with the diffusion constants determined for the ab initio Na_{93}^+ at temperatures $T = 248$, 262 and 274 K. The diffusion constant is calculated in the case of Na_{93}^+ over the last time period of 1 ps. The melting region of Na_{55}^+ starts at about 300 K seen as a fast increase of the diffusion constant as a function of temperature. Large values of the diffusion constant for Na_{93}^+, and fast increase with T strongly indicate that the melting

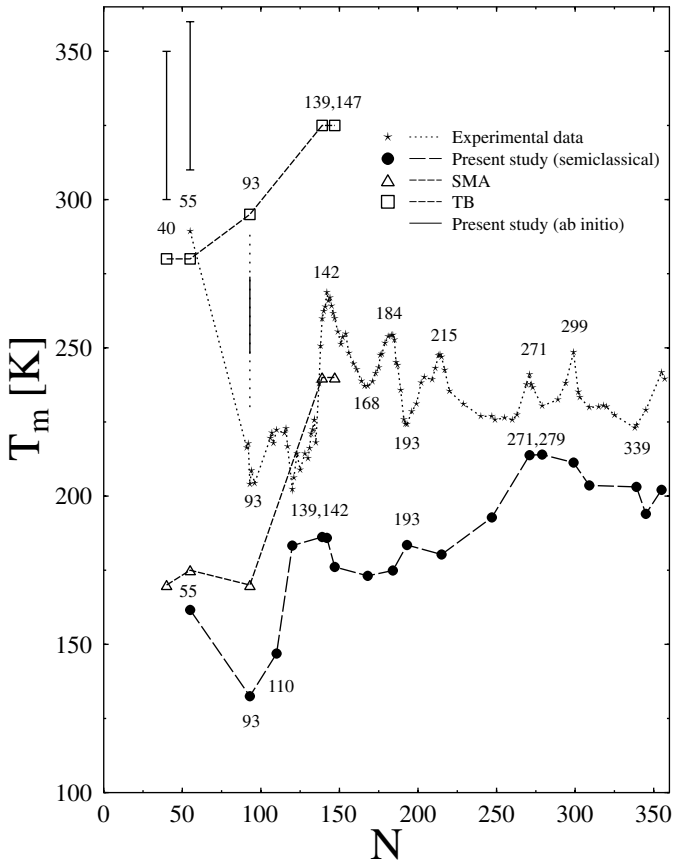

Fig. 2. Melting temperature of sodium clusters as a function of cluster size. Our results are marked with a filled circle, the experimental results of Haberland et al. [3,11,13] are marked with a star, and the results by Calvo et al. [10] are marked with an open triangle (SMA) and an open square (TB). The points have been connected with each other using different linetypes but the lines do not tell how the melting temperature behaves between the points.

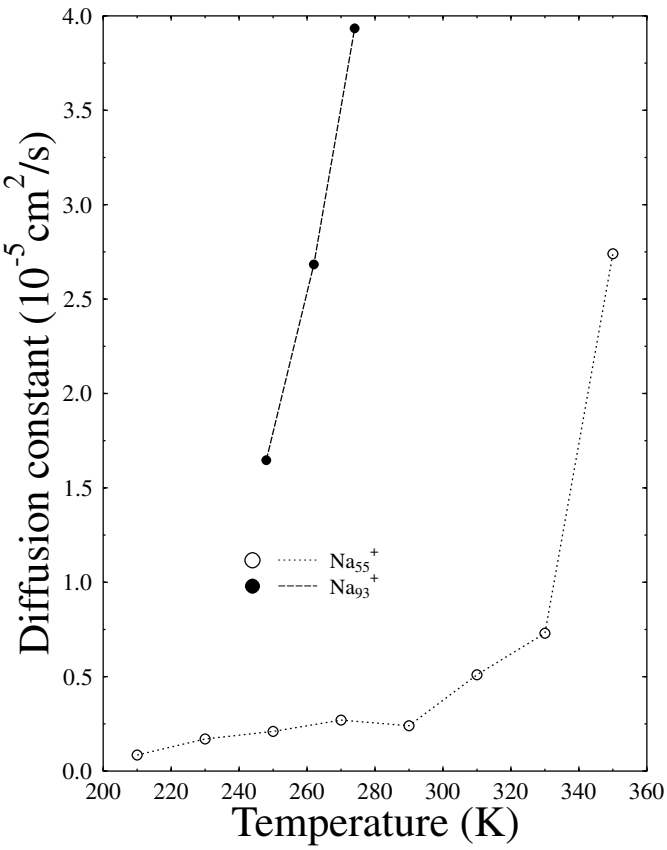

Fig. 3. The diffusion constant as a function of the temperature. Open circles and filled circles represent the simulation results for Na_{55}^+ and Na_{93}^+, respectively.

temperature of Na_{93}^+ is below the lowest simulated temperature 248 K, in good agreement with the experimental findings.

Figure 4 shows the Kohn-Sham single-electron energy eigenvalues of Na_{93}^+ in temperature 274 K as a function of time. The electronic structure exhibits clear energy gaps at 2, 8, 18, 20, 34, 58, 92, and 138, consistent with the spherical jellium picture [41]. All these gaps, including the HOMO-LUMO gap at 92, remain open during the simulation, showing that the liquid cluster stays electronically magic. It is interesting to note that the experimentally observed magic number 40 is not seen as a clear gap. Indeed, the result suggests that for a spherical system, 34 actually is a more clear electronic magic number than 40, as well-known from spherical jellium calculations. The fact that 40 is the true magic number in experiments is a manifestation of a strong octupole deformation of this cluster size as suggested first by Hamamoto et al. [53] and demonstrated by ab initio simulations by Rytkönen et al. [2]. The octupole deformation opens a large HOMO-LUMO gap for the size 40 and makes that an important magic number

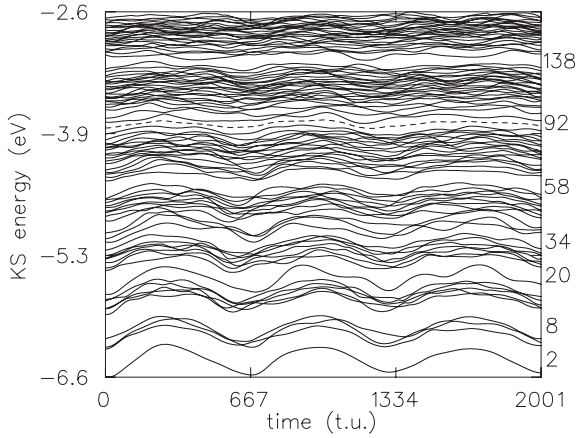

Fig. 4. The Kohn-Sham single-electron energy eigenvalues of Na_{93}^+ at temperature 274 K as a function of time. The discontinuity line presents the Fermi energy.

instead of the size 34. In the case of simulated Na_{93}^+, the electronic structure favors a spherical shape and the gap at 40 electrons stays small. The present ab initio simulations together with our earlier studies clearly show that the liquid sodium clusters stay electronically magic, suggesting that the electronic shell structure could have a role in the melting process.

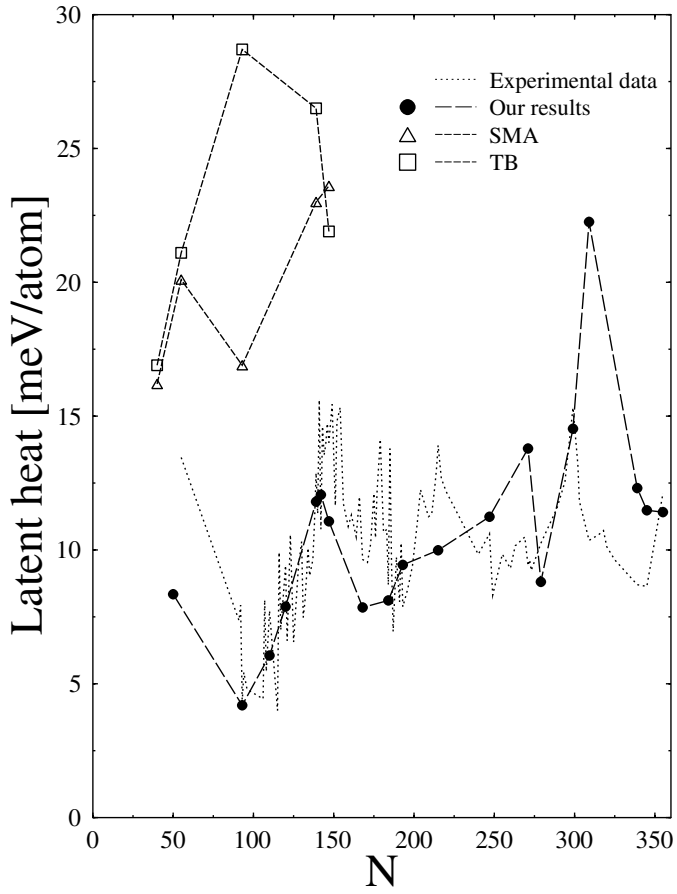

Fig. 5. Latent heat of sodium clusters as a function of cluster size. Our results are marked with a filled circle, the experimental results of Haberland et al. [5,13,25] are marked with a star, and the results by Calvo et al. [10] are marked with an open triangle (SMA) and an open square (TB) (SMA uses the same potential as ours). The points have been connected to each other with different lines but the lines do not tell how the latent heat behaves between the points.

The latent heat of melting as a function of cluster size determined both experimentally and with both our and Calvo's [10] simulation method is shown in Figure 5. The curve shows maxima at cluster sizes $N = 55$, 142, 271 and 309. The experimental latent heat of fusion for $N = 55-139$ behaves similarly as our results [5,13,25], but again, the results for the larger sizes do not correlate.

Comparing the latent heat of fusion (Fig. 5) to the melting temperature (Fig. 2) determined with the semi-classical method, we find out that the behaviors from 55 to 120, from 139 to 193, and from 215 to 271 are similar in these two quantities. In the size range from 279 to 309, the peak in the latent heat curve is shifted from that of T_{melt} toward of the icosahedral shell closing. Good correlation between these two quantities can be seen in Figure 7. Generally, it seems that the melting temperature and latent heat of fusion are both sensitive to same factors. The cluster size $N = 309$ is interesting, because the latent heat of fusion is relatively high (Fig. 7). On the other hand, the latent heat of size $N = 279$ is smaller than expected on the basis of the melting temperature.

The experimental results of Schmidt et al. indicate that melting temperatures and latent heats of fusion could have correlation with each other [25]. They also observed that the maxima in the latent heat curve seem to be shifted from the maxima for the melting temperature towards of the icosahedral shell closing. Ab initio calculations for a 55 atom cluster showed that the melting temperature and the latent heat of fusion are both a little higher than the experimental values [8], so they correlate with each other in a similar manner as the experimental values.

However, our latent heats do not correlate with the results of Calvo and Spiegelmann [10]. Calvo et al. predict two different variations for the latent heat and no correlation with T_{melt}. These calculations also overestimate the latent heat over the whole size range. The reason for this can lie in a method different from ours used to analyse the latent heat.

The half width of the heat capacity peak (given by c in Eq. (5)) as a function of cluster size is presented in Figure 6a. The curve shows pronounced maxima in the cases of 93, 120, 215 and 345 and minima in the cases of 142, 279 and 355. The width and the height (not shown) of the peak correlate with each other. The heat capacity peak gets higher and narrower in the cases of 142, 279 and 299 atoms. The width of the heat capacity peak generally decreases with increasing N, but is not a monotonic function of N.

Figure 6b presents the binding energy difference for sodium clusters as a function of size. Binding energy, by itself, is found to be a monotonically increasing function of cluster size for this model. To see the possible regions of increased stability, it is convenient to subtract a smooth size dependence from the energy. This can be obtained by fitting the binding energies to $E_{\rm ave}^{binding} = a+bN^{-1/3}+cN^{-2/3}+d/N$, where a, b, c and d are the fitting parameters. After the fit, we get values $a = 1.203$ eV, $b = -2.152$ eV, $c = 5.315$ eV and $d = -8.501$ eV. The highest maxima at sizes $N = 55$, 135 and 297, agree with those obtained also by Northby [46] and are caused by the icosahedral geometry.

Figure 1 demonstrates that the specific heats for the solid and the liquid phases are almost constant, which is in agreement with the experimental results of reference [25]. The average value of heat capacity for the solid phase is 0.275 meV/K per atom and the average value of the heat capacity for the liquid phase is 0.343 meV/K. These values are slightly higher than the experimental values 0.245 meV/K and 0.303 meV/K for bulk solid and liquid, respectively [25]. These values are comparable with the Dulong-Petit value 0.26 meV/K.

4 Conclusion

The molecular dynamics simulations with a tight-binding potential show that the melting temperature of small

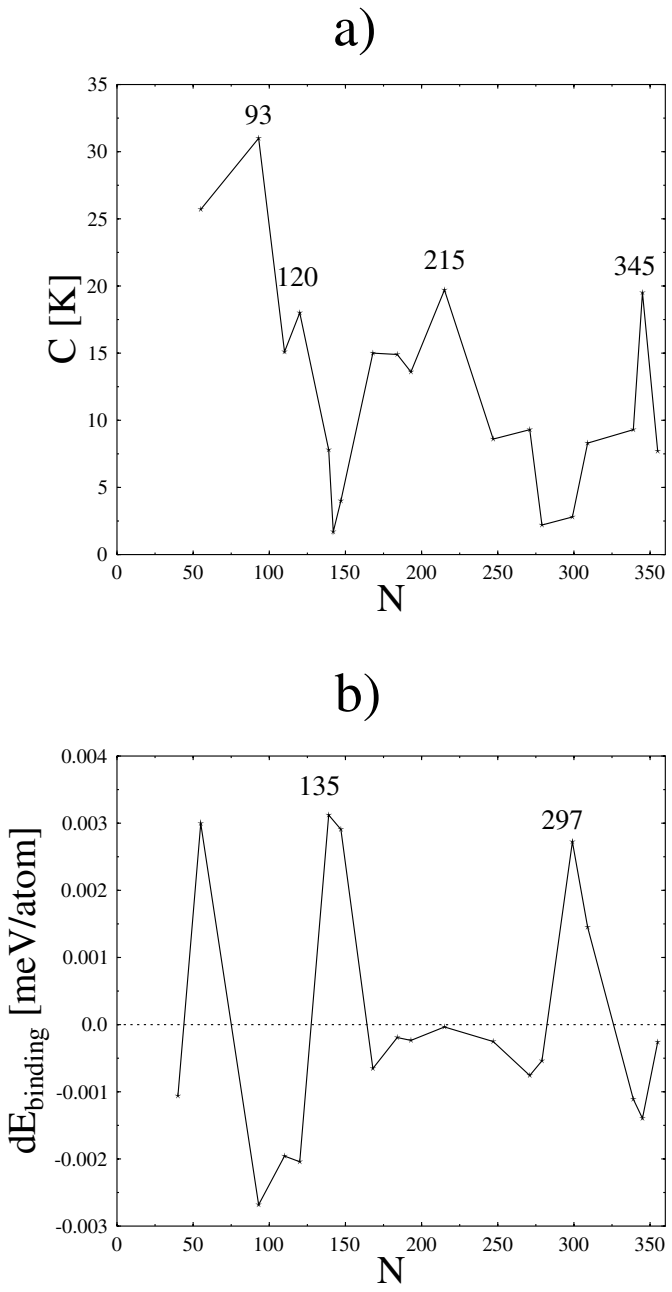

Fig. 6. (a) The half width of the heat capacity peak (c) versus cluster size. (b) The binding energy difference of sodium cluster as a function of size. Both the half width and the binding energy difference have been calculated by using semiclassical molecular dynamics simulations.

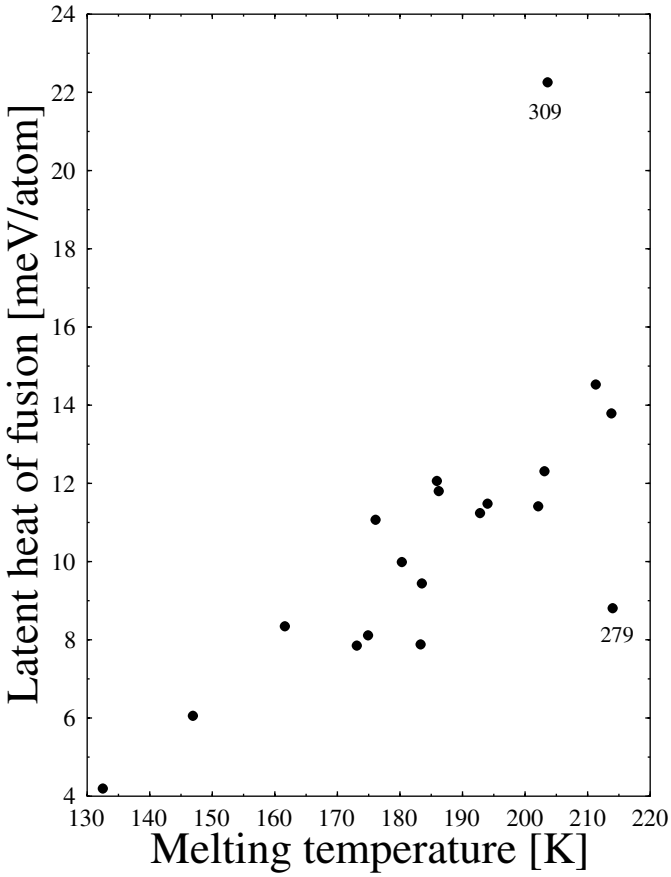

Fig. 7. Correlation between latent heat of fusion and melting temperature calculated using semiclassical molecular dynamics simulations.

sodium clusters is a non-monotonous function of cluster size. For the sizes 55, 93 and 147, the qualitative dependence is similar to that observed experimentally. However, for larger clusters the simulated size-dependence of the melting temperature does not follow the experimental results.

The ab initio molecular dynamics methods was used to simulate the Na_{93}^+ cluster at three different temperatures. The results showed that the cluster melts at a temperature below 240 K, in agreement with the experimental melting temperature of about 210 K. Our earlier simulations showed that the melting temperature of Na_{55}^+ was between 300 and 350 K, in fair agreement with the experimental result of 290 K. Both these simulations indicate that the ab initio molecular dynamics could give accurate results for the melting temperatures of sodium clusters, if enough computation power would be available.

The ab initio simulations for Na_{93}^+ showed that even in the liquid state the cluster stays electronically magic. The HOMO-LUMO gap stays open even though the individual single-electron energy levels oscillate quite strongly with time. The present result also confirms the earlier finding [2] that the 40 electron sodium cluster is made magic by a strong octupole deformation.

We would like to thank Hellmut Haberland and his research group for sending us results prior to publication. We also wish to thank H. Häkkinen, M. Schmidt and T. Hippler for valuable discussions. Parallel computers of CSC-Scientific Computing were used for the computations. This work has been supported by the Academy of Finland under the Finnish Centre of Excellence Programme 2000-2005 (Project No. 44875, Nuclear and Condensed Matter Programme at JYFL).

References

1. S.L. Lai, J.Y. Gou, V. Petrova, G. Ramanath, L.H. Allen, Phys. Rev. Lett. **77**, 99 (1996)
2. A. Rytkönen, H. Häkkinen, M. Manninen, Phys. Rev. Lett. **80**, 3940 (1998)
3. M. Schmidt, R. Kusche, W. Kronmûller, B. von Issendorff, H. Haberland, Phys. Rev. Lett. **79**, 99 (1997)
4. F. Ercolessi, W. Andreoni, E. Tosatti, Phys. Rev. Lett. **66**, 911 (1991)
5. M. Schmidt, R. Kusche, B. von Issendorff, H. Haberland, Nature **393**, 238 (1998)
6. A.A. Shvartsburg, M.F. Jarrold, Phys. Rev. Lett. **85**, 2530 (2000)
7. F. Calvo, F. Spiegelmann, Phys. Rev. Lett. **82**, 2270 (1999)
8. A. Rytkönen, H. Häkkinen, M. Manninen, Eur. Phys. J. D **8**, 93 (2000)
9. T.L. Beck, J. Jellinek, R.S. Berry, J. Chem. Phys. **87**, 545 (1986)
10. F. Calvo, F. Spiegelmann, J. Chem. Phys. **112**, 2888 (2000)
11. M. Schmidt, R. Kusche, W. Kronmüller, B. von Issendorff, H. Haberland, in The Physics and Chemistry of Clusters, *Proceedings of Nobel Symposium* **117** (World Scientific, Singapore, 2001), p. 326
12. D.J. Wales, R.S. Berry, J. Chem. Phys. **92**, 4283 (1989)
13. R. Kusche, Th. Hippler, M. Schmidt, B. von Issendorff, H. Haberland, Eur. Phys. J. D **9**, 1 (1999)
14. L.T. Hill, *Thermodynamics of small systems* (Benjamin, New York, 1963)
15. V. Bonačić-Koutecký, J. Jellinek, M. Wiechert, P. Fantucci, J. Chem. Phys. **107**, 6321 (1997)
16. H.-P. Cheng, R.S. Berry, Phys. Rev. A **45**, 7969 (1992)
17. F. Celestini, R.J. Pellenq, P. Bordarier, B. Rousseau, Z. Phys. D **37**, 49 (1996)
18. R.N. Barnett, U. Landman, Phys. Rev. B **44**, 3226 (1991)
19. A. Rytkönen, M. Manninen, Eur. Phys. J. D **23**, 352 (2003)
20. D.J. Wales, R.S. Berry, Phys. Rev. Lett. **73**, 2875 (1994)
21. R.S. Berry, J. Jellinek, G. Natanson, Phys. Rev. A **30**, 919 (1984)
22. R.E. Kunz, R.S. Berry, Phys. Rev. Lett. **71**, 3987 (1993)
23. J. Jellinek, T.L. Beck, R.S. Berry, J. Chem. Phys. **84**, 2783 (1985)
24. H. Matsuoka, T. Hirokawa, M. Matsui, M. Doyma, Phys. Rev. Lett. **69**, 297 (1992)
25. M. Schmidt, J. Donges, Th. Hippler, H. Haberland, Phys. Rev. Lett. **90**, 103401 (2003)
26. A. Rytkönen, S. Valkealahti, M. Manninen, J. Chem. Phys. **108**, 5826 (1997)
27. C.L. Cleaveland, W.D. Luedtke, U. Landman, Phys. Rev. B **60**, 5056 (1991)
28. S. Valkealahti, M. Manninen, Comput. Mat. Sci. **1**, 123 (1993)
29. I.J. Gilvarry, Phys. Rev. **103**, 1700 (1956)
30. W.A. Curtis, N.W. Ashcroff, Phys. Rev. Lett. **56**, 2775 (1986)
31. T.P. Martin, U. Näher, H. Schaber, U. Zimmermann, J. Chem. Phys. **100**, 2322 (1993)
32. F. Calvo, P. Labastie, J. Phys. Chem. B **102**, 2051 (1998)
33. J.P.K. Doye, D.J. Wales, Phys. Rev. B **59**, 2292, (1999)
34. J.P.K. Doye, D.J. Wales, J. Chem. Phys. **111**, 11070 (1999)
35. N. Ju, A. Bulgac, Phys. Rev. B **48**, 2721 (1993)
36. J.A. Reyes-Nava, I.L. Garzón, K. Michaelian, Phys. Rev. B **67**, 165401 (2003)
37. A. Aguado, J.M. López, J.A. Alonso, M.J. Stott, J. Phys. Chem. B **105**, 2386 (2001)
38. A. Aguado, L.M. Molina, J.M. López, J.A. Alonso, Eur. Phys. J. D **15**, 221 (2001)
39. A. Rytkönen, H. Häkkinen, M. Manninen, Eur. Phys. J. D **9**, 451 (1999)
40. T.P. Martin, Phys. Rep. **273**, 199 (1996)
41. W.A. de Heer, Rev. Mod. Phys. **65**, 611 (1993)
42. Y. Imry, Phys. Rev. B **21**, 2042 (1980)
43. P. Labastie, R.L. Whetten, Phys. Rev. Lett. **65**, 1567 (1990)
44. A. Rytkönen, M. Manninen, J. Chem. Phys. **113**, 4647 (2000)
45. C. Rey, L.J. Gallego, J. Garcia-Rodeja, J.A. Alonso, M.P. Iniguez, Phys. Rev. B **48**, 8253 (1993)
46. J.A. Northby, J. Chem. Phys. **87**, 6166 (1987)
47. L. Verlet, Phys. Rev. **159**, 98 (1967)
48. W.G. Hoover, Phys. Rev. A **31**, 1695 (1985)
49. Y. Li, E. Blaisten-Barojas, D.A. Papaconstantopoulos, Phys. Rev. B **57**, 15519 (1998)
50. R.N. Barnett, U. Landman, Phys. Rev. B **48**, 2081 (1993)
51. L. Kleinman, D.M. Bylander, Phys. Rev. Lett. **48**, 1425 (1982)
52. N. Troullier, J.L. Martins, Phys. Rev. B **43**, 1993 (1991)
53. I. Hamamoto, B.R. Mottelson, H. Xie, X.Z. Zhang, Z. Phys. D **21**, 163 (1991)
54. J.P. Neirotti, F. Calvo, D.L. Freeman, J.D. Doll, J. Chem. Phys. **112**, 10340 (2000)
55. D.D. Frantz, J. Chem. Phys. **115**, 6136 (2001)